Nonlinear Fault Ride-Through of Grid Forming Converters with Power Synchronization Control

Yousef Khayat
Dept. of Electrical Engineering, Chalmers University of Technology
Göteborg, Sweden
yousefkh@chalmers.se

Peiyuan Chen
Dept. of Electrical Engineering, Chalmers University of Technology
Göteborg, Sweden
peiyuan.chen@chalmers.se

Massimo Bongiorno
Dept. of Electrical Engineering, Chalmers University of Technology
Göteborg, Sweden
massimo.bongiorno@chalmers.se

***Abstract*—Grid-forming (GFM) converters, recognized as a key mechanism for providing frequency and voltage support to weak power grids, confront a significant challenge in maintaining stability during severe voltage dips and providing fault ride-through (FRT) capability. To tackle this challenge, this study first uncovers why GFM converters lose their synchronization during the current limit operation mode subjected to grid-side voltage dips. Then, a nonlinear analytical control law for power synchronization control (PSC) based GFM power converters to enhance their FRT capability during grid side severe voltage dips is provided. The effectiveness of the proposed methods is shown through time-domain EMT simulation results, and it is investigated for grids with different short circuit ratios (SCRs).**

***Index Terms*—Fault ride-through, grid-forming power converters, weak grids, nonlinear control**

I. Introduction

The global energy shift towards renewables is resulting in a higher contribution of power converters, which prone the grid to be weaker, and posing stability challenges for the grid. Grid-forming (GFM) control is the preferred solution considered for addressing weak grid challenges, they behave like a controllable voltage source with slow changes behind an impedance, while, an active power controller is responsible for ensuring the synchronized operation of the power converter. This growing integration of renewables demands the need for fault ride-through (FRT) capability [1]. It obligates the power-generating units to stay connected to the grid and keep their stable operation during grid faults. Without it, there is a risk of losing synchronization among power generators, potentially resulting in a system collapse [2].

Similar to synchronous generators (SGs), FRT analysis for GFMs employs tools like the power–angle (P–δ) curve, phase portrait, and equal area criteria (EAC); however, over current limitations of power converters (which can only tolerate 1.2–1.5 times) brings more complexity for conventional FRT analysis of GFMs [3]. This over-current transient refers to the inherent behavior of a GFM's voltage source behind impedance, and grid faults can readily trigger undesired converter overcurrents and pose potential risks for instability.

Most existing methods used for FRT of GFMs include modifying the reference active power reference by decreasing accelerating power and/or injecting additional reactive power to enhance the output voltage during grid faults. The main challenge with these methods lies in quantifying the changes in power references, i.e., selecting values for some control parameters that necessitate some prior knowledge about the grid parameters, authors utilized load angle [4], [5], and a frequency-based threshold [6] approach for reference power modifying. Some other methods focus on adaptive tuning of the control parameters in the active power control loop for both the inertial and damping gains by considering the acceleration and deceleration modes similar to a conventional SG [7], [8], or employing the methods that switch between the acceleration to/in deceleration mode with a negative unit gain to avoid LOS [9]–[11], or switches to do the synchronization according to the reactive power loop's dynamics [12]. Limiting the current either by a virtual impedance/admittance [13] or by freezing/limiting the voltage control loop's integrator [14], or changing the priority of the power injection during the fault by fault-mode set point powers [15]–[19]. The main challenge of this group of solutions is that the converter loses most of its GFM capabilities. The last group of FRT solutions of GFMs provides an extra control loop for improving the large signal stability of the GFM, as the recent works presented in [20]–[22].

The aim of this paper is first to show P–δ curve of a power converter considering the current limitation issue subjected to grid-side voltage dips. Then, we have provided a step-by-step analytical Lyapunov-based control law design for ensuring the rotor-angle stability of power synchronization control (PSC) based GFMs during severe voltage dips. After showing the implementation mechanism of the provided nonlinear scheme, time-domain simulations are used to confirm the robustness of the proposed controller for grids with a wide range of different short circuit ratio (SCR) and different voltage dips.

II. Control Principle of PSC-GFM

System operators have recently outlined key required functions of the GFM capability; aiming to ensure that a GFM has to show a performance comparable to or better than an SG in supporting the grid during disturbances [1]. The first function is asked to create or form the system voltage by the GFM's internal voltage in amplitude, frequency, and phase angle, regardless of the connected loads or operation mode. Then, GFM is demanded to contribute during a short-circuit

fault, such that it should inject fault current up to its over-current capacity, as required by the grid code. In addition, during frequency disturbances, the GFM should provide an active-power response proportional to the rate-of-change-of-frequency (RoCoF), contributing to the total system inertia; subjected to the energy storage capacity and converter's power rating. Contributing to system damping and acting as a sink against harmonics and unbalances in the grid voltage, and preventing adverse control interactions are the other required functions.

Figure 1 shows a GFM with a power synchronization control (PSC) mechanism for the active power loop and a voltage control loop (VCL). In this way, the synchronization of the converter system with the AC grid relies on transient power transfer. As it can be seen, the PSC is responsible for calculating θ_{GFM} as the phase-angle of the virtual back electromotive force (EMF), and E as the amplitude of the virtual back EMF is controlled by the VCL. The PSC utilizes the proportional gain k_{PSC} and the VCL utilizes the integral gain k_v to generate E and θ_{GFM} according to

$$E = E_0 + \overbrace{(k_v/s)}^{G_{vcl}(s)}\,(v_{ref} - |v_c| - k_d Q_e) \tag{1a}$$

$$\dot{\theta}_{GFM} = \omega_0 + \underbrace{(k_{PSC})}_{G_{APL}(s)}\,(P_{ref} - P_e) \tag{1b}$$

where E_0, ω_0, k_d, are the set point value of the back EMF, set point angular frequency, reactive power droop, and reference active power, respectively. Measured powers are calculated by carrying out the variables from the $\alpha\beta$-frame into dq-frame using θ_{GFM} as

$$P_e = v_d^c i_d^o + v_q^c i_q^o \tag{2a}$$

$$Q_e = v_q^c i_d^o - v_d^c i_q^o \tag{2b}$$

Design requirements for a robust tuning of k_{PSC} can be found in [23]. A virtual admittance (VA) is then utilized for generating the reference currents in the form of

$$i^*_{N-Lim} = \frac{v_{emf} - v^c_{\alpha\beta}}{R_v + s\,L_v} \tag{3}$$

where R_v and L_v are the resistive and inductive parts of VA, respectively; $v_{emf} = E\angle\theta_{GFM}$ is the virtual back-EMF vector, and $v^c_{\alpha\beta}$ is the capacitor voltage vector in the point of measurement (PoM). The non-limited reference current i^*_{N-Lim} is then limited for the safe operation purposes of the power converter; which by a circular current limiter can be formulated as

$$i^*_{Lim} = \sigma i^*_{N-Lim}, \tag{4a}$$

$$\sigma \equiv \{1,\ I_M/\| i^*_{N-Lim} \|\} \tag{4b}$$

where i^*_{Lim} is the limited reference current, and I_M is the maximum current that the converter can tolerate during overcurrents. A proportional-resonant (PR) controller as the current controller (CC) calculates the reference voltage for the modulation unit, as shown in Fig. 1.

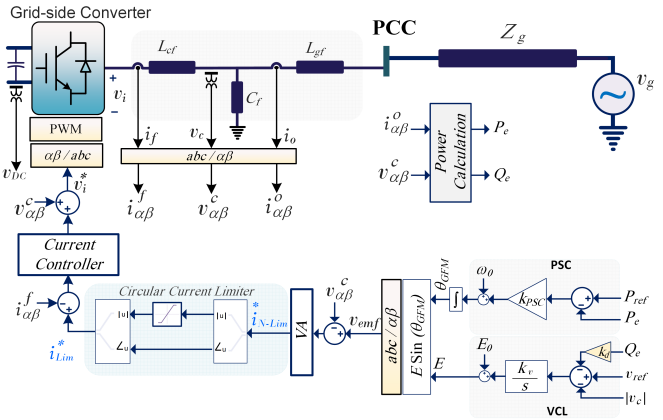

Fig. 1. The overall configuration of a connected PSC-GFM system to an external Thevenin-modeled grid with the block diagrams of its different control loops.

Assuming an inductive characteristic for the system, the transferred active and reactive powers from the power converter with v_{emf} to the grid Thevenin voltage with $v_g = V_g\angle\theta_g$ at the sending end in quasi-steady state can be approximately determined as

$$P = \frac{3}{2}\frac{EV_g sin(\delta)}{x_t} \tag{5a}$$

$$Q = \frac{3}{2}\frac{E^2 - EV_g cos(\delta)}{x_t} \tag{5b}$$

where $\delta = \theta_{GFM} - \theta_g$ is the load angle, x_t represents the total output reactance between v_{emf} and v_g.

III. GFM Angle Instability During Current Saturation

The key contributor to the angle stability challenge in the GFM converters during voltage dips is an active-power reference that surpasses the power transfer limit that grid conditions allow during a fault or in the post-fault steady-state. For example, equation (5a) illustrates that the active-power transfer between the GFM's back EMF and the grid voltage is directly proportional to the product of E and V_g. Consequently, a voltage dip leads to a reduced active-power transfer capability, regardless of how the magnitude of the virtual back-EMF is adjusted in response to the voltage dip. In addition, the effect of the current saturation unit can be considered for a power transfer limit study. To do so, let's consider that the virtual back-EMF v_{emf} located behind the virtual impedance Z_{vir} connected to the Thevenin equivalent of grid with v_g and Z_g. Ignoring the system losses, and assuming that the load angle displacement between v_{emf} and v_g is donated by δ, the per-unit (pu) converter current i_c in steady state in the synchronous reference frame (SRF) aligned with v_{emf} can be formulated by

$$i_c = \frac{v_{emf} - v_g}{jx_t} = \frac{E\angle\delta - v_g\angle 0}{x_t} = \frac{E\sin(\delta) + j(v_g - E cos(\delta))}{x_t} \tag{6}$$

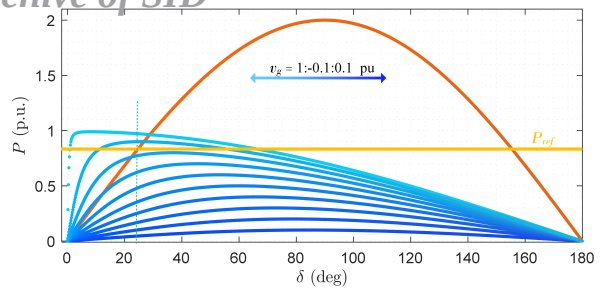

Fig. 2. $P-\delta$ curves with and without circular current saturation unit when $I_M = 1$ pu. The red curve shows P in (5a) for a grid with $x_t = 0.5$ pu. The blue curves are P_e^{lim} in (8) for current saturated cases when $v_g = 1 : -0.1 : 0.1$ pu with the same x_t.

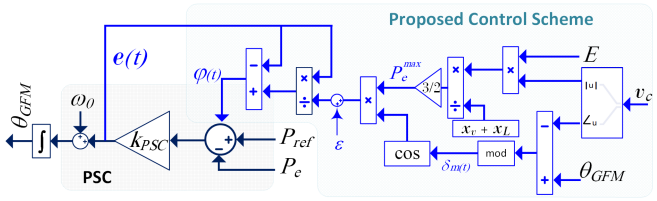

Fig. 3. Implementation of the proposed nonlinear Lyapunov FRT solution, $x_v + x_L$ is the total impedance between the back-EMF voltage v_{emf} and capacitor filter's voltage v_c.

where x_t stands for the total reactance between v_{emf} and v_g. Considering a circular current limitation, one can find the saturated injected current is as

$$\begin{aligned} i_c^{lim} &= I_M \times \frac{i_c}{||i_c||} \\ &= I_M \times \frac{E\sin(\delta) + j(v_g - E\cos(\delta))}{\sqrt{E^2 + v_g^2 - 2E \cdot v_g \cdot \cos(\delta)}}. \end{aligned} \tag{7}$$

The saturated active power can thus be calculated through

$$\begin{aligned} P_e^{lim} &= Re\{E\angle\delta \times conj(i_c^{lim})\} \\ &= \frac{E \cdot v_g \cdot \sin(\delta) I_M}{\sqrt{E^2 + v_g^2 - 2E \cdot v_g \cdot \cos(\delta)}}. \end{aligned} \tag{8}$$

Equ. (8) shows that P_e^{lim} is a function of E, v_g, δ, and the current saturation level I_M. In this regard, Fig. 2 illustrates the $P-\delta$ curves with and without circular current saturation during different voltage dip transients when the set-point active power $P_{ref} = 0.8$ pu; and a conceptual stability analysis can be done as like as the equal area criteria (EAC) for the power converters considering its current saturation's effect on power transfer limit during different voltage dips.

IV. Proposed Control Mechanism

In order to derive a Lyapunov control law for keeping the rotor-angle stability, let's recall the PSC's frequency dynamics, as

$$\omega_{PSC} = \omega_0 + \dot{\delta}(t) \tag{9a}$$

$$\dot{\delta}(t) = k_{PSC}(P_{ref} - P) \tag{9b}$$

Other dynamics are neglected due to their decoupled bandwidth. Inserting (5a) in (9b), results in

$$\dot{\delta}(t) = k_{PSC}(P_{ref} - \frac{3}{2}\frac{v_{emf}v_g}{x_v + x_L + x_G}sin(\delta)). \tag{10}$$

Now, let's introduce

$$\delta_m(t) = \theta_{GFM}(t) - \theta_c(t), \tag{11}$$

where $\theta_c(t)$ is thephase angle of the measured voltage of the capacitor, by this way, a measurable $\delta_m(t)$ can be accessible which is the phase displacement between the converter's back EMF voltage and the measured voltage of the capacitor in the LCL filter location. In this way, inspired from eq. (10), the rotor-angle dynamics between the back-EMF and the measured capacitor voltage can be rewritten as

$$\dot{\delta}_m(t) = k_{PSC}(P_{ref} - \frac{3}{2}\frac{v_{emf}v_c}{x_v + x_L}sin(\delta_m)) \tag{12}$$

Assuming the control input $\varphi(t)$ is going to be designed through the Lyapunov candidate, and is added to eq. (12) as below

$$\dot{\delta}_m(t) = k_{PSC}(P_{ref} - \overbrace{(\frac{3}{2}\frac{v_{emf}v_c}{x_v + x_L})}^{P_e^{max}}\sin(\delta_m)) + \varphi(t). \tag{13}$$

Now, let's formulate a tracking control issue, such that the transient error $e(t)$ can be expressed as

$$e(t) = P_{ref} - P_e^{max}\sin(\delta_m(t)) \tag{14}$$

By defining the Lyapunov candidate $\mathcal{V}(t) = 0.5e(t)^2$, its derivative with respect to time can be expressed as

$$\begin{aligned} \dot{\mathcal{V}}(t) &= \dot{e}(t)e(t) \\ &= (\dot{P}_{ref} - P_e^{max}\dot{\delta}_m(t)\cos\delta_m(t))e(t). \end{aligned} \tag{15}$$

By inserting (13) in the above equation, one can find

$$\begin{aligned} \dot{\mathcal{V}}(t) = (\dot{P}_{ref} - P_e^{max}[k_{PSC}(P_m - P_e^{max}\sin\delta_m(t)) \\ + \varphi(t)]\cos\delta_m(t))e(t). \end{aligned} \tag{16}$$

In order to design the control signal $e(t)$ to stabilize the dynamics shown in (13), $\dot{\mathcal{V}}(t)$ need to be always negative. To this end, let's assume that $\dot{\mathcal{V}}(t) = -e^2(t)$, reformulating (16) leads to

$$(\dot{P}_{ref} - P_e^{max}[e(t) + \varphi(t)]\cos\delta_m(t))e(t) = -e^2(t). \tag{17}$$

Calculating $\varphi(t)$ in (17) leads to

$$\varphi(t) = \frac{\dot{P}_{ref} + e(t)}{P_e^{max}\cos\delta_m(t)} - e(t). \tag{18}$$

Control law (18) [1] shows a stabilized control signal for keeping the synchronization of (12) between the back-EMF v_{emf} with the grid and its robust performance during severe grid voltage dips are shown in the next section. Figure 3 shows the implementation mechanism of the control law (18), while it is assumed that the $\dot{P}_{ref} = 0$.

[1] In order to avoid algebraic loop errors during situations where the denominator converges to zero, ε as a small positive term can be employed to prevent division by zero as shown in Fig. 3.

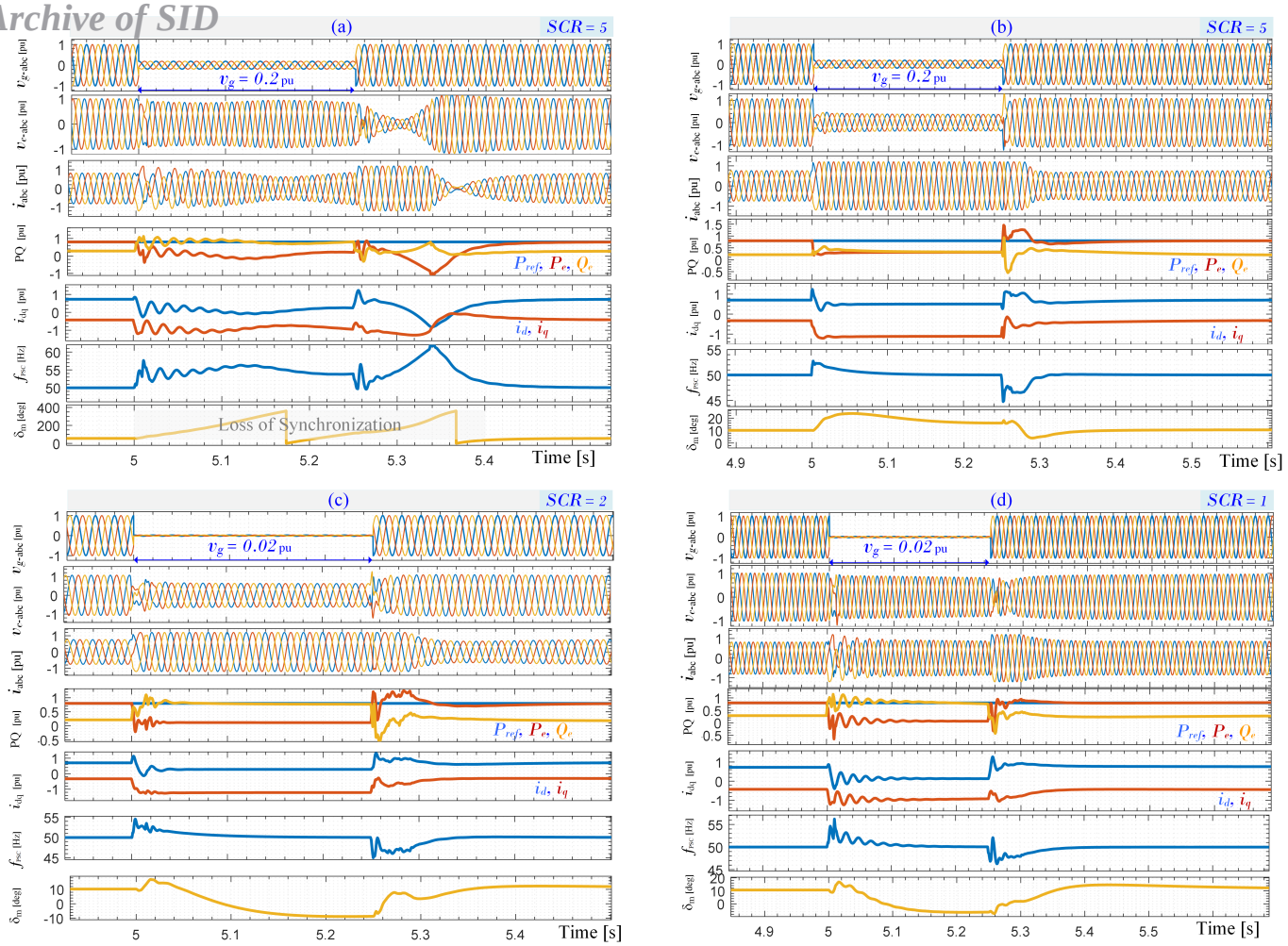

Fig. 4. From top to bottom of each subplot: three-phase grid voltages v_{g-abc}, three-phase GFM's capacitor output filter voltages v_{c-abc}, three-phase GFM's reference limited currents, active and reactive powers, dq reference currents, PSC's frequency and phase displacement between vectors of v_{emf} and v_c. (a) dynamic performance during grid voltage dip from 1 p.u. to 0.2 p.u., without proposed nonlinear Lyapunov FRT scheme for a grid with SCR 5 (instable case) (b) dynamic performance during grid voltage dip from 1 p.u. to 0.2 p.u., with the proposed nonlinear Lyapunov FRT scheme for a grid with SCR 5, (c) dynamic performance during grid voltage dip from 1 p.u. to 0.02 p.u., with the proposed nonlinear Lyapunov FRT scheme for a grid with SCR 2, and (d) dynamic performance during grid voltage dip from 1 p.u. to 0.2 p.u., with the proposed nonlinear Lyapunov FRT scheme for a grid with SCR 1. The duration of the fault for all cases is 250 ms.

V. Verifications and Results

To demonstrate the effectiveness of the suggested nonlinear control law for ensuring the angle-stability of PSC-GFMs during severe voltage dips, this section provides real-time simulation results for a grid-connected PSC with parameters outlined in Table II. The objective is to assess the performance of the PSC under severe voltage dips for grids with SCR $\in$ [1 - 10].

The results, both with and without the proposed nonlinear Lyapunov scheme, are depicted in Fig. 4(a)-(d), where the grid voltage drops from 1 p.u. to 0.2 p.u. at t = 5 s and recovers back to 1 p.u. at t = 5.25 s in Fig. 4(a) and (b), and voltage drops from 1 p.u. to 0.02 p.u. as a extremely severe fault with the same duration in Fig. 4(c) and (d). The grid SCR for each case is shown. The reference active power remains unchanged before, during, and after the fault for all the cases. The current limitation for all the cases is set to 1.2 pu, as can be seen from the 3rd subplot in Figs.(a)-(d).

In Fig. 4(a), when the voltage of the grid with SCR = 5 drops to 0.2 p.u. at t = 5 s, the load angle δ starts to increase as the active power output from the VSC is lower than its reference value. In this scenario, the proposed nonlinear control scheme scheme is not activated. Consequently, the active power output does not exceed its reference value to create a deceleration torque. As a result, the VSC loses synchronization with the grid and two swings can be seen from the last subplot of Fig. 4(a).

Figure 4(b)-(d) illustrates the corresponding results with the proposed nonlinear Lyapunov scheme. During the grid voltage dip for all three cases with different SCRs, the PSC can keep stable operation, without angle swinging, the control signal $\varphi(t)$ stabilizes the power mismatch among P_{ref} and P_e by adding appropriate deceleration power. Additionally, the

TABLE I. TEST SYSTEM PARAMETERS

Symbol	Description	Value
S_n	Rated power	7.5 kVA
V_{base}	Base l-l voltage	400 V (rms)
I_M	Saturation level	1.2 pu
f_0	Nominal frequency	50 Hz
f_{sw}	Switching frequency	10 kHz
C_f	Filter capacitor	0.07 pu
L_{cf}	Converter-side inductor	0.075 pu
L_{gf}	Grid-side inductor	0.075 pu
SCR	Short circuit ratio	5 - 1 pu

TABLE II. CONTROL PARAMETERS

Control Loop	Symbol	Description	Value
CC	k_{p-cc}	Proportional gain	12 Ω
	k_{r-cc}	Resonant gain	1000 Ω /s
VA	R_v	Virtual resistive	0.1 pu
	L_v	Virtual inductive	0.3 pu
APL	k_{PSC}	PSC gain	0.0012 rad/(s.W)
VCL	k_v	Voltage control gain	3.2 pu
	k_d	Reactive power droop	0.24 Volt/Var
Lyapunov	ε	Denominator offset term	0.01 —

reactive power injection is automatically done by the voltage source behavior of the GFM.

VI. CONCLUSIONS

This paper has shown the limited power transfer issue for grid-connected power converters during voltage dips, where reference set-point active power exceeds the amount of power limit injection that grid conditions allow and leads to instability. This motivated us to provide an analytical Lyapunov-based FRT solution for PSC-GFM power converters in this paper. The nonlinear control law has been extracted from the power-angle dynamics between the voltage vectors of the back-EMF voltage of the GFM and the measured voltage at the location of the LCL filter of the power converter. The design procedure has relied on local measurements and parameters, with no need for knowledge of the grid conditions, guaranteeing a robust performance for PSC-GFMs against extremely severe voltage dips.

REFERENCES

[1] P. Imgart, M. Beza, M. Bongiorno, and J. R. Svensson, "An overview of grid-connection requirements for converters and their impact on grid-forming control," in *2022 24th European Conference on Power Electronics and Applications (EPE'22 ECCE Europe)*. IEEE, 2022, pp. 1–10.

[2] M. Naderi, Y. Khayat, Q. Shafiee, F. Blaabjerg, and H. Bevrani, "Dynamic modeling, stability analysis and control of interconnected microgrids: A review," *Applied Energy*, vol. 334, p. 120647, 2023.

[3] A. Narula, P. Imgart, M. Bongiorno, M. Beza, J. R. Svensson, and J.-P. Hasler, "Voltage-based current limitation strategy to preserve grid-forming properties under severe grid disturbances," *IEEE Open Journal of Power Electronics*, vol. 4, pp. 176–188, 2023.

[4] J. Erdocia, A. Urtasun, and L. Marroyo, "Power angle–frequency droop control to enhance transient stability of grid–forming inverters under voltage dips," *IEEE Journal of Emerging and Selected Topics in Power Electronics*, 2022.

[5] Y. Zhang, C. Zhang, R. Yang, M. Molinas, and X. Cai, "Current-constrained power-angle characterization method for transient stability analysis of grid-forming voltage source converters," *IEEE Transactions on Energy Conversion*, 2023.

[6] C. Collados-Rodriguez, D. W. Spier, M. Cheah-Mane, E. Prieto-Araujo, and O. Gomis-Bellmunt, "Preventing loss of synchronism of droop-based grid-forming converters during frequency excursions," *International Journal of Electrical Power & Energy Systems*, vol. 148, p. 108989, 2023.

[7] J. Alipoor, Y. Miura, and T. Ise, "Power system stabilization using virtual synchronous generator with alternating moment of inertia," *IEEE journal of Emerging and selected topics in power electronics*, vol. 3, no. 2, pp. 451–458, 2014.

[8] Y. Khayat, M. Naderi, H. Bevrani, and F. Blaabjerg, "Virtual inertia emulating in power electronic–based power systems," in *Control of Power Electronic Converters and Systems*. Elsevier, 2021, pp. 541–560.

[9] G. Wang, L. Fu, Q. Hu, C. Liu, and Y. Ma, "Transient synchronization stability of grid-forming converter during grid fault considering transient switched operation mode," *IEEE Transactions on Sustainable Energy*, 2023.

[10] H. Deng, Y. Qi, J. Fang, Y. Tang, and V. Debusschere, "A robust low-voltage-ride-through strategy for grid-forming converters based on reactive power synchronization," *IEEE Transactions on Power Electronics*, vol. 38, no. 1, pp. 346–357, 2022.

[11] H. Wu and X. Wang, "A mode-adaptive power-angle control method for transient stability enhancement of virtual synchronous generators," *IEEE Journal of Emerging and Selected Topics in Power Electronics*, vol. 8, no. 2, pp. 1034–1049, 2020.

[12] K. Li, P. Cheng, L. Wang, X. Tian, J. Ma, and L. Jia, "Improved active power control of virtual synchronous generator for enhancing transient stability," *IET Power Electronics*, vol. 16, no. 1, pp. 157–167, 2023.

[13] Z. Jin and X. Wang, "A dq-frame asymmetrical virtual impedance control for enhancing transient stability of grid-forming inverters," *IEEE Transactions on Power Electronics*, vol. 37, no. 4, pp. 4535–4544, 2021.

[14] S. Dadjo Tavakoli, E. Prieto-Araujo, O. Gomis-Bellmunt, and S. Galceran-Arellano, "Fault ride-through control based on voltage prioritization for grid-forming converters," *IET Renewable Power Generation*, vol. 17, no. 6, pp. 1370–1384, 2023.

[15] L. Zhang, L. Harnefors, and H.-P. Nee, "Power-synchronization control of grid-connected voltage-source converters," *IEEE Transactions on Power systems*, vol. 25, no. 2, pp. 809–820, 2009.

[16] M. G. Taul, X. Wang, P. Davari, and F. Blaabjerg, "Current limiting control with enhanced dynamics of grid-forming converters during fault conditions," *IEEE Journal of Emerging and Selected Topics in Power Electronics*, vol. 8, no. 2, pp. 1062–1073, 2019.

[17] B. Fan and X. Wang, "Fault recovery analysis of grid-forming inverters with priority-based current limiters," *IEEE Transactions on Power Systems*, 2022.

[18] E. Rokrok, T. Qoria, A. Bruyere, B. Francois, and X. Guillaud, "Transient stability assessment and enhancement of grid-forming converters embedding current reference saturation as current limiting strategy," *IEEE Transactions on Power Systems*, vol. 37, no. 2, pp. 1519–1531, 2021.

[19] A. H. Etemadi and R. Iravani, "Overcurrent and overload protection of directly voltage-controlled distributed resources in a microgrid," *IEEE Transactions on Industrial Electronics*, vol. 60, no. 12, pp. 5629–5638, 2012.

[20] P. Imgart, A. Narula, M. Bongiorno, M. Beza, and J. R. Svensson, "A cascaded power controller for robust frequency ride-through of grid-forming converters," in *2022 IEEE Energy Conversion Congress and Exposition (ECCE)*. IEEE, 2022, pp. 1–8.

[21] M. Naderi, Y. Khayat, Q. Shafiee, F. Blaabjerg, and H. Bevrani, "Robust synchronization of multiple converter-based weak microgrids for smooth interconnection," *IEEE Transactions on Power Systems*, 2023.

[22] B. Fan and X. Wang, "A lyapunov-based nonlinear power control algorithm for grid-connected vscs," *IEEE Transactions on Industrial Electronics*, vol. 69, no. 3, pp. 2916–2926, 2021.

[23] L. Harnefors, M. Hinkkanen, U. Riaz, F. M. Rahman, and L. Zhang, "Robust analytic design of power-synchronization control," *IEEE Transactions on Industrial Electronics*, vol. 66, no. 8, pp. 5810–5819, 2018.